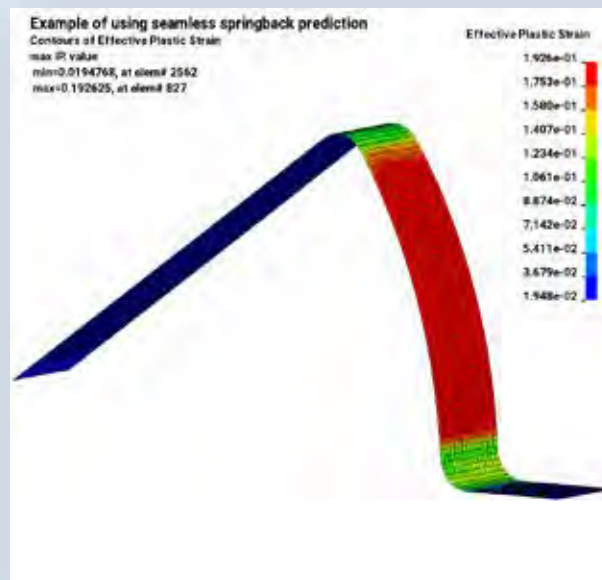


# FEA Information Engineering Journal



**Article: The final effective plastic strain contours  
of the workpiece running with 10 CPUs in MPP.**

# FEA Information Engineering Journal

---

**Editors: Yanhua Zhao - Dilip Bhalsod – Marsha Victory**

## **Aim and Scope**

FEA Information Engineering Journal (FEAIEJ™) is a quarterly published online journal to cover the latest Finite Element Analysis Technologies. The journal aims to cover previous noteworthy published papers and original development updates. All published papers are peer reviewed in the respective FEA engineering fields.

Consideration is given to all aspects of technically excellent written information without limitation on length. All submissions must follow guidelines for publishing a paper, or periodical. If a paper has been previously published, FEAIEJ requires written permission to reprint, with the proper acknowledgement given to the publisher of the published work.

Reproduction in whole, or part, without the express written permission of FEA Information Engineering Journal, or the owner of the copyright work, is strictly prohibited. FEAIEJ welcomes unsolicited topics, ideas, and articles.

Monthly publication is limited to no more than five papers or informational articles of interest, either reprint, or original. Papers will be archived on [www.feaij.com](http://www.feaij.com)

For information on publishing a paper original or reprint contact [editor@feaij.com](mailto:editor@feaij.com) Subject line: Journal Publication

*Cover:*

Fig. Figure 3.

*Article:* The final effective plastic strain contours of the workpiece running with 10 CPUs in MPP.

*Livermore Software Technology Corporation*

# FEA Information Engineering Journal

## TABLE OF CONTENTS

---

**Publications are © to the authors and are informational short subject publishings**

All contents are copyright © to the publishing company, author or respective company. All rights reserved.

- 01 New features of 3D adaptivity in LS-DYNA  
W. Hu, LSTC
  
- 02 New Feature: Defining Hardening Curve in LS-DYNA®  
Xinhai Zhu, Li Zhang, Yuzhong,  
LSTC
  
- 03 Improvement of Mesh Fusion in LS-DYNA  
Houfu Fan, Xinhai Zhu, Li Zhang and Yuzhong Xiao,  
LSTC
  
- 04 Representative Volume Element (RVE) analysis using LS-DYNA  
C.T. Wu, W. Hu  
LSTC
  
- 05 Improvement of Sandwich Structure Part Adaptivity in LS-DYNA  
Xinhai Zhu, Houfu Fan, Li Zhang and Yuzhong Xiao  
LSTC
  
- 06 New Inflator Models in LS-DYNA®  
Kyoung-Su Im, Zeng-Chan Zhang, and Grant O. Cook, Jr.  
LSTC

## New features of 3D adaptivity in LS-DYNA

W. Hu      LSTC

The 3D remeshing in adaptivity is defined by the keyword \*CONTROL\_REMESHING, where the two important parameters, RMIN and RMAX, are the minimum and maximum mesh size in the re-meshing. The internal remesher of LS-DYNA uses these two values globally for all adaptive parts. In many applications, users may need more flexibility on defining the mesh size for different parts of the model. This short paper presents two new features: run-time control and \*DEFINE\_ADAPTIVE\_BOX in 3D adaptivity.

By setting IADPFCTRL=1 (\*CONTROL\_ADAPTIVE, Card4, the 7<sup>th</sup> flag), users are able to perform run-time control on 3D adaptivity through control files in the following manners:

- (1) Trigger additional adaptive step in run time
- (2) Setup a special adaptive step with the option of manual remeshing by users
- (3) For multiple adaptive parts, define remeshing parameters individually

In the current implementation, there are two control files: adapt.fc1 and adapt.fc2. They can be automatically generated by LS-DYNA if they are not pre-defined.

The file adapt.fc1 has three control parameters: C1 is the overall switch for this module; C2 defines the time for the next additional adaptive step; C3 is the switch for manual remeshing. The detail can be found in the following three examples:

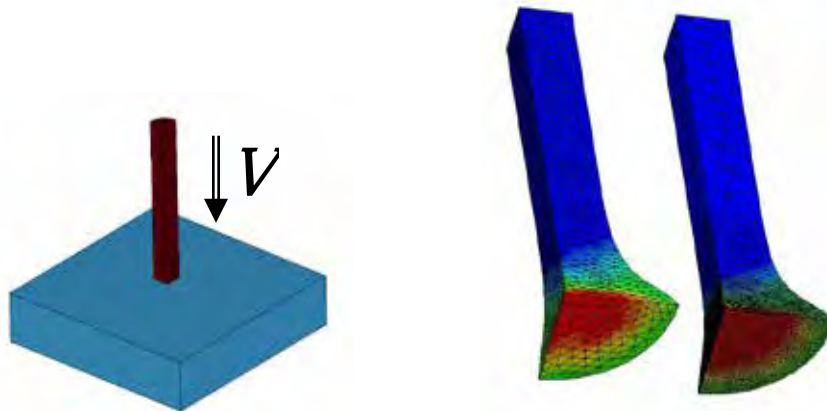
- (1) 1, 0.0, 0: C1=1 to turn on run-time control; C2=0.0 to start additional adaptivity immediately; C3=0 to turn off manual remeshing
- (2) 1, 0.01, 0: C2=0.01 to start additional adaptivity at the time 0.01
- (3) 1, 0.01, 3: C3=3 to turn on manual remeshing of the adaptive part 3 in the additional adaptive step at time 0.01

In this case, LS-DYNA is paused and the mesh information of part 3 is output into a keyword file, named user.mesh. Users can either manually change the mesh or use CAD software to generate a new mesh and then save into the same file. LS-DYNA continues the analysis by users setting C1=-1 in adapt.fc1.



reduce the overall computational cost. All of these differences in defining adaptivity for different parts can be made in adapt.fc2.

The 3D adaptivity in LS-DYNA has the capability to automatically perform dynamic mesh refinement based on the curvature of contact surfaces. In addition to that, \*DEFINE\_ADAPTIVE\_BOX is now supported for users to define multiple boxes in space with different definitions of remeshing mesh size. In the card 2 of this keyword, users can specify the adaptive part ID (PID), the minimum mesh size (BRMIN) and the maximum mesh size (BRMAX) so that, within the box defined in the card 1, all the mesh from this part is remeshed using BRMIN/BRMAX instead of the global RMIN/RMAX. The following shows a Taylor bar impact simulation using 3D adaptivity (a quarter model), where the standard remeshing is compared to the one with three remeshing boxes defined by \*DEFINE\_ADAPTIVE\_BOX. The results show that the second one is able to capture the high-gradient field with much finer mesh and at the same time achieve the optimal performance with better distribution of mesh size.



\* Dr. W. Hu graduated from the department of civil engineering in UCLA in 2007, and joined LSTC in 2009. He has been working on the research and development of adaptivity and meshless methods.

## New Feature: Defining Hardening Curve in LS-DYNA®

Xinhai Zhu, Li Zhang, Yuzhong Xiao  
LSTC

### INTRODUCTION

This keyword defines material hardening curve based on a few commonly used material hardening laws. Weighted combinations of the hardening laws are also made possible. The load curve ID, which represents stress-strain curve defined here, can be referenced in the load curve ID used by a specific material model. This feature is applicable to all material models with a hardening curve defined by a load curve using \*DEFINE\_CURVE.

### MAIN FEATURES

With this keyword, a user can define five different types of hardening laws (ITYPE 1 through ITYPE 5), and to combine one of the laws (ITYPE 1) with other laws (ITYPE 2 through ITYPE 5) with weighting factors. There are currently five types of hardening laws implemented as follows,

ITYPE=1: Swift power law in the form of:

$$\sigma = K(e_0 + \epsilon_p)^n,$$

where  $\sigma$  is true effective stress,  $e_0$  is the elastic strain at the initial yield point,  $K$  is a strength coefficient,  $\epsilon_p$  is true effective plastic strain,  $n$  is the work hardening coefficient. Input variables defined as follows:

$$P1 = K, \quad P2 = e_0, P3 = n.$$

ITYPE=2: Voce law in the form of:

$$\sigma = \sigma_0 + R_{sat}(1.0 - e^{-zeta\epsilon_p}),$$

where  $\sigma_0$  is the initial yield stress,  $R_{sat}$  is the stress differential between  $\sigma_0$  and the saturated stress,  $zeta$  is a strain coefficient. Input variables defined as follows:

$$P1 = \sigma_0, P2 = R_{sat}, P3 = zeta, P4: \text{hardening curve contributing weighting factor.}$$

ITYPE=3: Voce law in the form of:

$$\sigma = A - B e^{-C\epsilon_p},$$

where  $A, B, C$  are material constants. Input variables defined as follows:

$$P1 = A, P2 = B, P3 = C, P4: \text{hardening curve contributing weighting factor.}$$

ITYPE=4: Hockett-Sherby law in the form of:

$$\sigma = A - B e^{-C\epsilon_p^H},$$

where  $A, B, C$ , and  $H$  are material constants. Input variables defined as follows:

$P1 = A, P2 = B, P3 = C, P4 = H, P5$ : hardening curve contributing weighting factor.

ITYPE=5: Stoughton-Yoon hardening law in the form of:

$$\sigma = A - B e^{-C * \epsilon_p^m} + D * \epsilon_p,$$

where  $A, B, C, m$  and  $D$  are material constants, and,

$0 < m < 1.0$ , and,

$D \geq 0.0$

Input variables defined as follows:

$P1 = A, P2 = B, P3 = C, P4 = M, P5 = D, P6$ : hardening curve contributing weighting factor.

According to Stoughton-Yoon, “with the exception of metals exhibiting Yield Point Elongation (YPE) effects, this function can represent the stress-strain response for BOTH mild and AHSS steel AND aluminum, from the initial yield point, throughout the small strain range, up to the highest strains realized in bulge tests”.

Note that if  $D = 0.0$ , this function reduces to the Hockett-Sherby law (ITYPE 4). Also note that if  $m = 1.0$  and  $D = 0.0$ , this function reduces to one of the Voce law (ITYPE 3).

ITYPE=11: A weighted combination of ITYPE=1 (first card) and any of the ITYPE=2, 3, or 4 (second card). ITYPE 1 becomes ITYPE 11 when P4 (a contributing weighting factor) is defined in the first card. The variable P4 (for ITYPE 2 and 3), P5 (for ITYPE 4) or P6 (for ITYPE 5) also needs to be defined in the second card, see an example below.

## EXAMPLE

The following example shows a hardening curve (LCID 90903) will be created, which is the combination of 50% of Swift power law (ITYPE 1) and 80% of Hockett-Sherby law (ITYPE 4). In Figure 2, from a single element uniaxial tension test (Figure 1) in LS-DYNA, the hardening curves of the power law (ITYPE 1), Hockett-Sherby law (ITYPE 4) and the weighted combination of the two laws are shown. The weighted combination matches that from the hand-calculation.

```
*MAT_037
$      MID      RO      E      PR      SIGY      ETAN      R      HLCID
      1 7.900E-09 2.070E+05      0.30
*DEFINE_CURVE_STRESS
$-----1-----2-----3-----4-----5-----6-----7-----8
$ ITYPE=1: power law. P1=K, P2=n, P3=e0, P4=0.5.
$ ITYPE=4: Hockett-Sherby law. P1=A, P2=B, P3=C, P4=H, P5=0.8.
$      VOCE: sigma=A-B*exp(-C*eps**H)
$      LCID      TYPE      P1      P2      P3      P4      P5
      90903      11      350.0      0.22      0.01      0.5
      90903      4      162.2      72.2      4.34      1.2      0.8
```

Figure 3 shows an example of Stoughton-Yoon hardening law under uniaxial tension from LS-DYNA, compared with result from hand-calculation.

## REVISION INFORMATION:

This feature is available starting from Revision 113640. ITYPE 5 (Stoughton-Yoon) is available starting from Revision 114803.

## REFERENCE:

LS-DYNA User's Manual (draft).

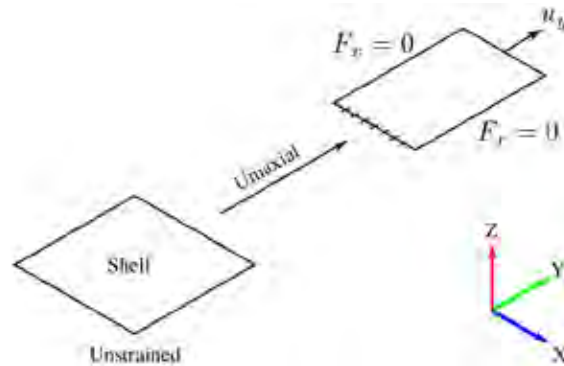


Figure 1 A single element in uniaxial tension

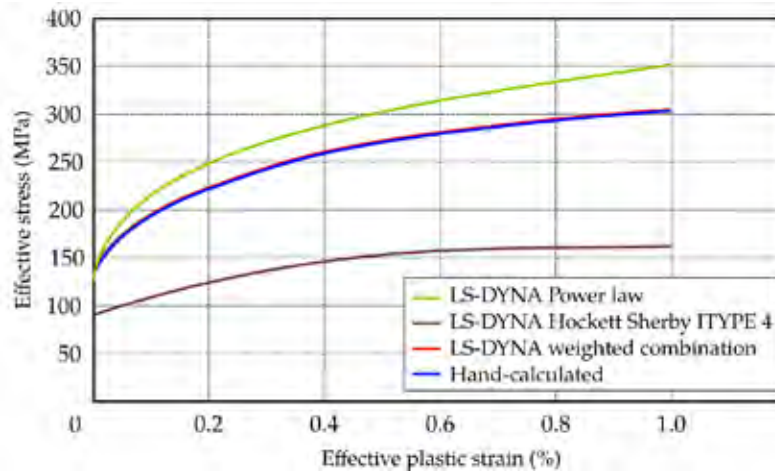
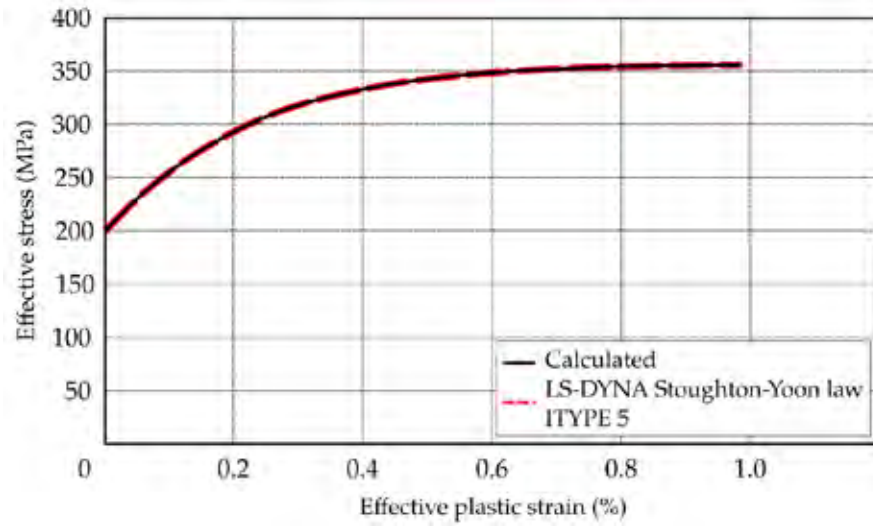


Figure 2 Resulting hardening curves from LS-DYNA comparison with hand-calculation.

$$\text{Power law: } \sigma = 350.0(0.01 + \epsilon_p)^{0.22},$$

$$\text{ITYPE 4 Voce law: } \sigma = 162.2 - 72.2e^{-4.34\epsilon_p^{1.2}},$$

$$\text{Weighted combination: } \sigma = 0.5 * 350.0(0.01 + \epsilon_p)^{0.22} + 0.8(162.2 - 72.2e^{-4.34\epsilon_p^{1.2}}).$$



**Figure 3 Comparison between Stoughton-Yoon results from LS-DYNA and hand- calculation.**

**( $A = 160.8024$ ,  $B = 71.109$ ,  $C = 4.5058$ ,  $M = 0.9989$ ,  $D = 0.8$ .)**

## Improvement of Mesh Fusion in LS-DYNA

Houfu Fan, Xinhai Zhu, Li Zhang and Yuzhong Xiao  
LSTC

### INTRODUCTION

To improve simulation efficiency, mesh fusion has been implemented in LS-DYNA® for a while. However, the implementation was only available in SMP, and its usage was very limited. Recently, mesh fusion has been successfully extended to MPP, and it can be activated with the existing keyword `*CONTROL_ADAPTIVE` through appropriate parameters `NCFREQ`, `ADPCTL`, `CBIRTH` and `CDEATH`.

In this work, it is demonstrated through benchmark examples that mesh fusion in MPP can reduce the simulation time, and maintain the accuracy of the forming process and the corresponding springback analysis.

### The Keyword `*CONTROL_ADAPTIVE`

Originally, adaptive fusion was implemented in SMP version. The adaptive fusion feature was turned off with a warning message displayed at the beginning of any simulations that require fusion in MPP. As of Revision 113867, mesh fusion in MPP is fully incorporated into the system.

The following keyword is the input to use the adaptive mesh fusion feature.

```
*CONTROL_ADAPTIVE
$  ADPFREQ   ADPTOL   ADPOPT   MAXLVL   TBIRTH   TDEATH   LCADP   IOFLAG
    2.00     4.0       2        3        0.0     70.0     0       1
$  ADPSIZE   ADPASS   IREFLG   ADPENE   ADPTH   MEMORY   ORIENT   MAXEL
    0.000000     1        0     5.000   0.0
$  IADPN90   IADPGH   NCFREQ   IADPCL   ADPCTL   CBIRTH   CDEATH   LCLVL
    -1        0        2        0        8.0     0.00     70.0
```

In the keyword, `NCFREQ` defines the fusion frequency, `ADPCTL` defines the fusion criterion, `CBIRTH` and `CDEATH` defines when the fusion starts and ends.

### Numerical Investigation

To test the performance of the new feature, a number of simulations were carried out using the NUMISHEET'93 Benchmark, as shown in Figure 1. For each case, a forming process is first conducted, followed by the corresponding springback analysis. The simulations are first carried out in MPP with the number of CPUs being 10. The performance comparison of the code with and without fusion is conducted. Specifically, we would like to check the differences in the simulation CPU time in the forming process, results in final springback angle, maximum effective plastic strain and minimum shell thickness in the workpiece with different number of CPUs running in MPP for cases with and without mesh fusion. As an illustration, the final mesh

sizes and shapes of the springback angles running with 10 CPUs in MPP with and without mesh fusion are given in Figure 2. The differences of the two final springback angles are calculated to be 8.1%. In addition, the contours of the final shell thickness and effective plastic strains are provided in Figures 3 and 4, respectively. The difference in the minimum shell thickness is 1.4% and in the maximum effective plastic strain is 1.7%. The simulation time reduction is around 25% (not shown in the Figure).

To have a better view on the performances of the feature over different number of CPUs running in MPP, the forming process and springback analysis were carried out with the number of CPUs ranging from 1 to 35. Time costs of the cases with and without mesh fusion are shown in Figure 5(a), and the corresponding springback angles are given in Figure 5(b). Time reduction, differences in springback angle, minimum shell thickness and maximum effective plastic strain are shown in Figures 6(a), 6(b), 7(a) and 7(b), respectively. One can see that the overall time reductions in the forming processes are in general greater than or equal to 25%. The differences in springback angles are kept within 10%; the differences in the minimum shell thicknesses and maximum effective plastic strains are always kept within 2%, which means they are not affected significantly by the mesh fusion.

## **CONCLUSION:**

The mesh fusion feature is successfully implemented in MPP and available for use. The fusion feature reduces the computation time notably (around 25%) and has little effects on formability analysis, such as thinning and effective plastic strain predictions. The difference in the corresponding springback results is also found to be smaller than 10%. The performance and accuracy studies can guide users in applying this new technology to a production simulation environment. Generally speaking, we should feel comfortable to use the fusion feature extensively in all formability related simulations since the leading indicators (shell thickness and effective plastic strain) affecting formability is hardly affected, but one can achieve a speed-up factor of 25% in simulation turnaround. In springback simulation, however, one should approach it with caution. One can apply the feature if the springback results are to be used for a quick and rough estimation. If the results are to be used for compensating dies and in deciding how much tools are going to be re-machined, then it may not be appropriate. The factor that people have higher expectation for springback simulation accuracy, now in the sub-millimeter when compared with physical scanned panel, should be taken into consideration when applying the feature in different scenarios.

In addition, the CPU time reduction can be affected by model of different sizes.

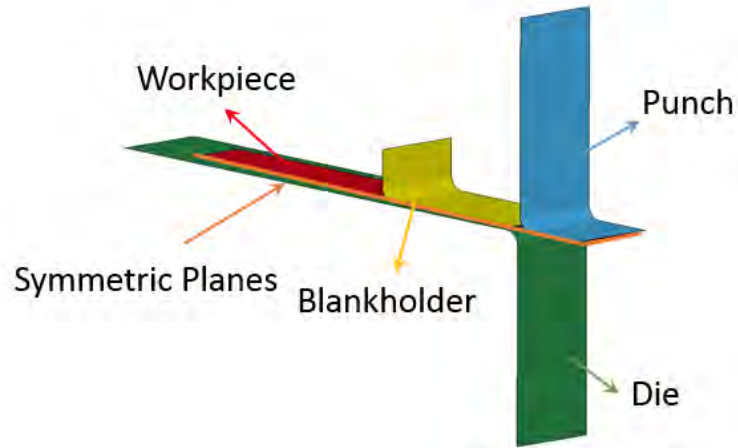


Figure 1. NUMISHEET'93 Benchmark: The punch, die and blankholder are rigid; the workpiece is discretized into shell elements. A forming process is conducted, followed by a springback analysis.

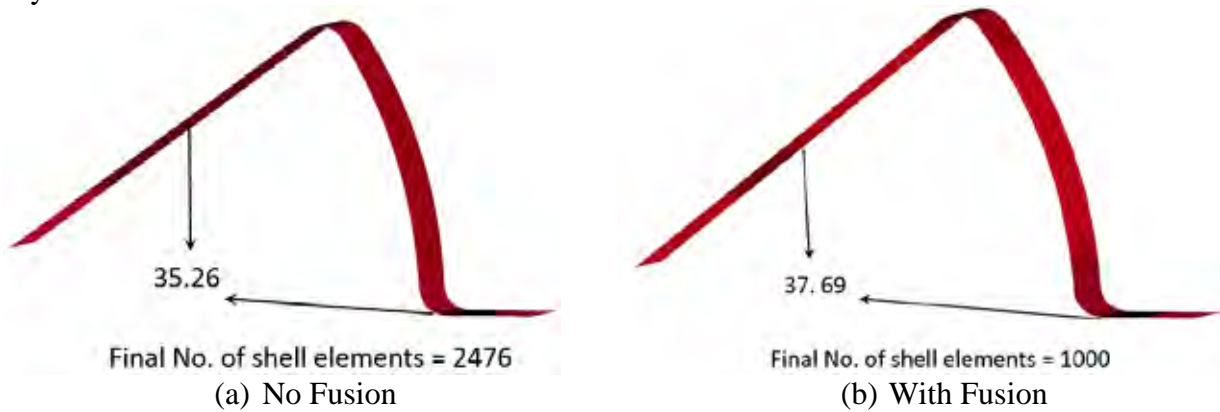
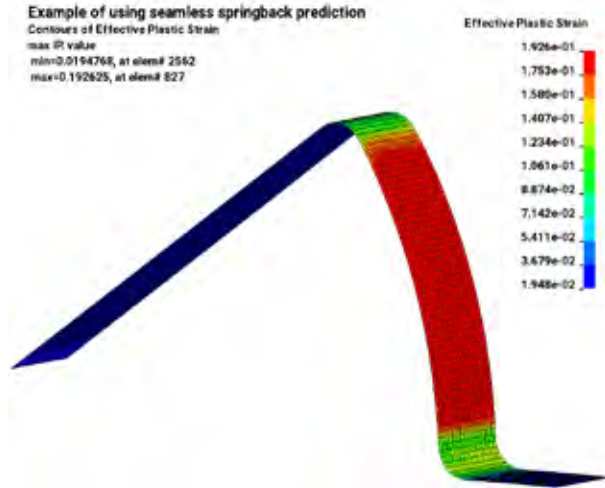
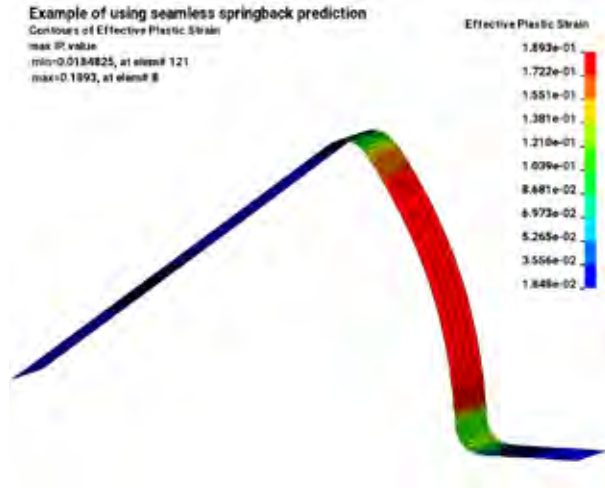


Figure 2. The final number of elements and springback angles of the workpiece running with 10 CPUs in MPP.

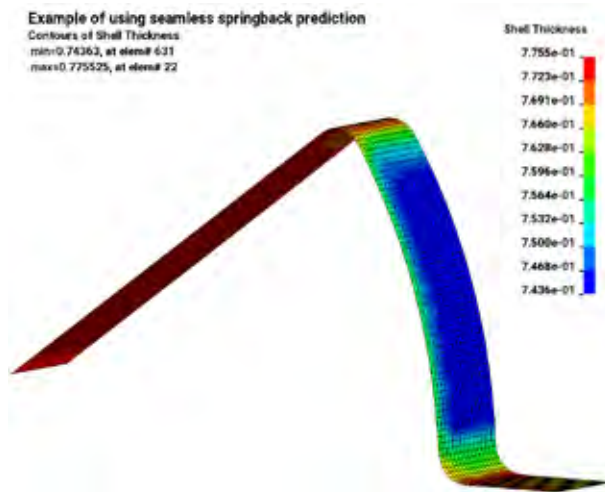


(a) No Fusion

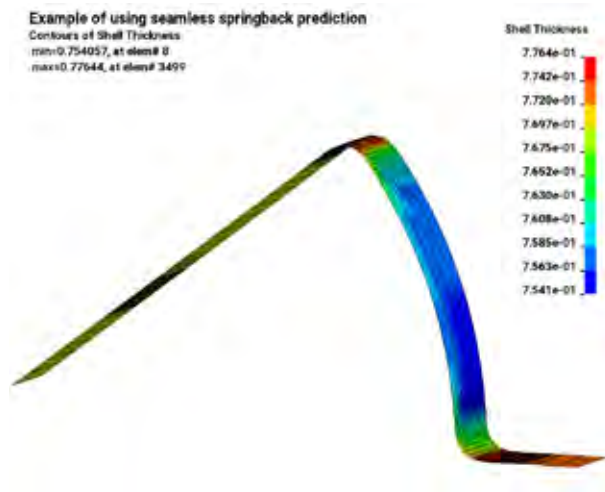


(b) With Fusion

Figure 3. The final effective plastic strain contours of the workpiece running with 10 CPUs in MPP.

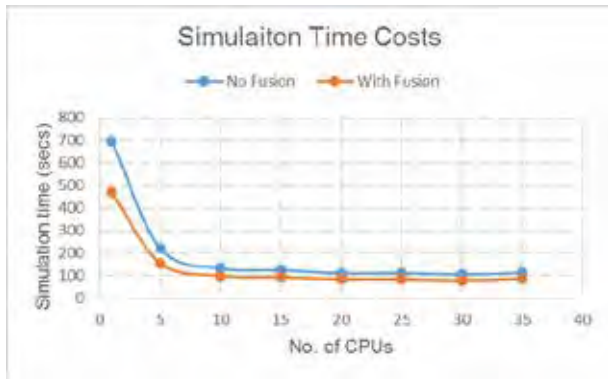


(a) No Fusion

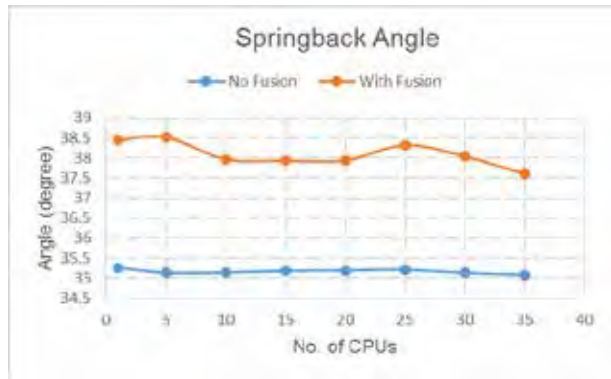


(b) With Fusion

Figure 4. The final shell thickness contours of the workpiece running with 10 CPUs in MPP.

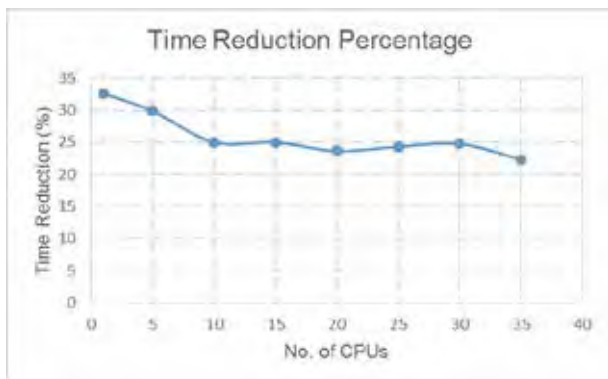


(a) Simulation Time

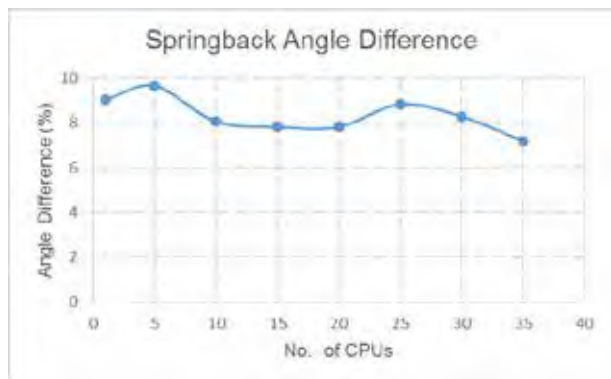


(b) Springback Angle

Figure 5. Comparisons of the simulation CPU time and springback angles in MPP with different number of CPUs, with and without mesh fusion.

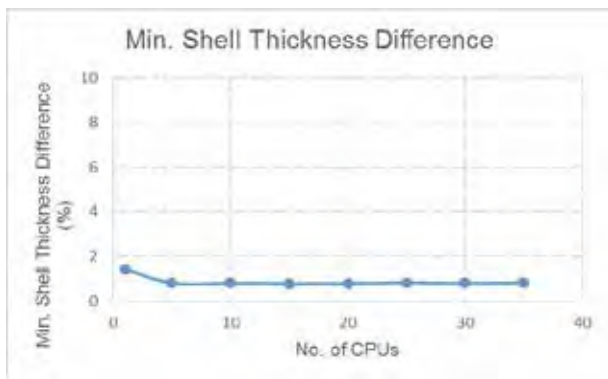


(a) Time Reduction

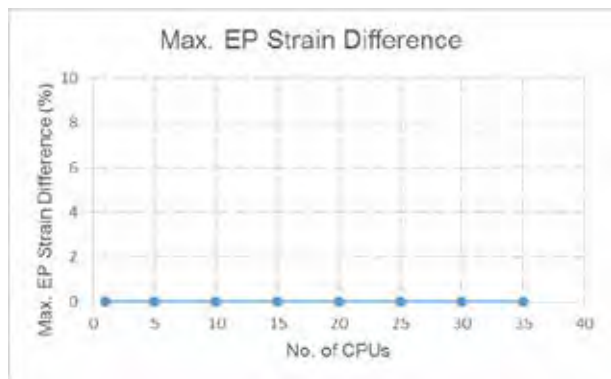


(b) Springback Angle Difference

Figure 6. Time reduction and springback angle differences in MPP with different number of CPUs, with and without mesh fusion.



(a) Min. Shell Thickness Difference



(b) Max. EP Strain Difference

Figure 7. Min. shell thickness and max. effective plastic strain differences in MPP with different number of CPUs, with and without mesh fusion.

**ACKNOWLEDGEMENT:**

The feature in this article was requested by BMW. Their valuable feedback during the development is highly appreciated.

**REVISION INFORMATION:**

Mesh fusion feature in MPP is available starting in Revision 113867.

# Representative Volume Element (RVE) analysis using LS-DYNA

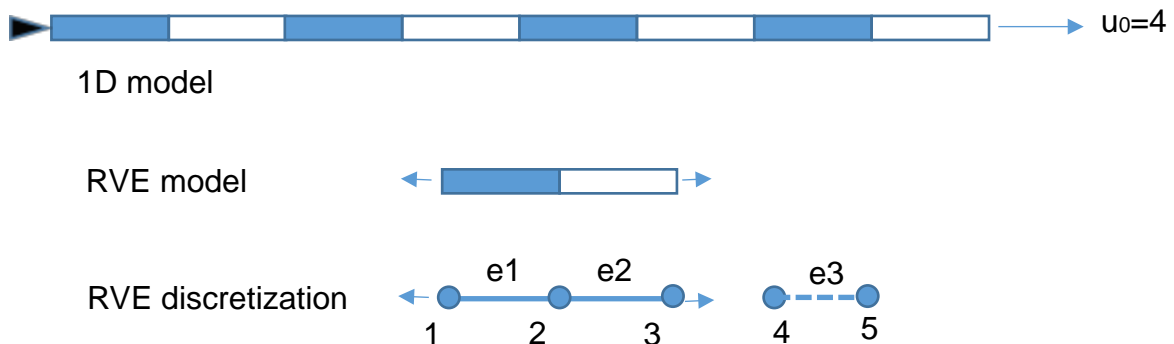
C.T. Wu, W. Hu      LSTC

With the emerging of new materials and novel manufacturing techniques, periodic structures in different scales are increasingly important in the real application, for example, battery arrays in cars, sub-scale structures in 3D printing products and all kinds of microstructures in material design analyses shown in the following pictures.



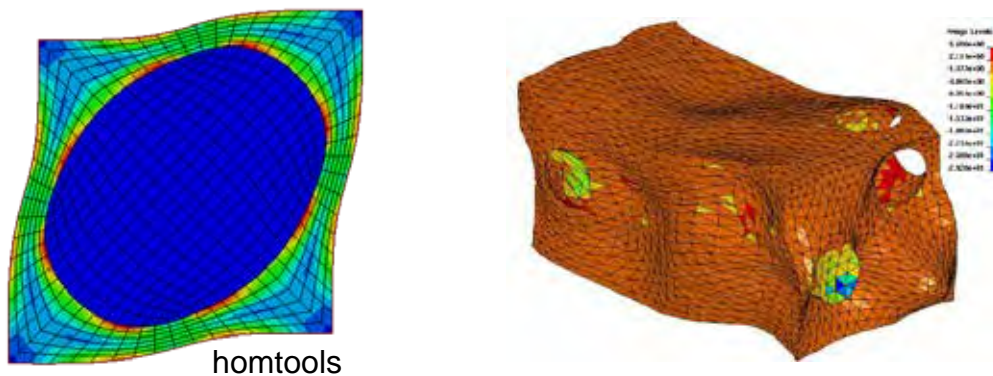
In the numerical simulation, it is very expensive to model the whole structure with a decent resolution for capturing fine details. For instance, when studying microstructure response under the macro level loading, the mesh size in the fine scale is orders of magnitude smaller than that of the macro structure. By introducing the assumption of periodicity, the large scale model can be simplified by RVE (Representative Volume Element) with periodic boundary conditions (PBC). In LS-DYNA, these PBC equations can be defined through `*CONSTRAINED_MULTIPLE_GLOBAL`. This short paper will focus on its use in RVE analysis and another keyword `*INCLUDE_UNITCELL` that simplifies the procedure of PBC definition.

First, let's talk about PBC equations using the following 1D model.



In this model, the left end is fixed and a prescribed displacement is imposed on the right

end. By introducing periodic assumption and element discretization, we obtain the FEM model with 3 nodes and two elements. The corresponding PBC is  $u_3 - u_1 = u_4$ , where the node 4 is the control point. It is required by \*CONSTRAINED\_MULTIPLE\_GLOBAL to define PBC by only nodal IDs and the coefficients. Since the node 4 is involved in PBC, we have to define a control element e3 with much higher stiffness and prescribe the displacement on the node 5 to indirectly impose the prescribed displacement boundary on RVE. You may have a question why not to define the conditions in a simple way like  $u_1 = 0$ ,  $u_3 = 1$ . This works in 1D but generally not in 2D and 3D. In the following figures, we can see that the deformation along RVE boundaries is not homogeneous so that we have to define PBC equations to enforce periodicity along with prescribed loading conditions.



The PBC equation  $u_3 - u_1 - u_4 = 0$  can be defined as follows:

\*CONSTRAINED\_MULTIPLE\_GLOBAL

1			Group ID of PBC equations
3			The number of nodes in the current PBC equation
1	1	-1	In every line, we need to list the nodal ID, the degree of freedom (DOF, 1:x; 2:y; 3:z), and the corresponding coefficient
3	1	1	
4	1	-1	

Here are two remarks :

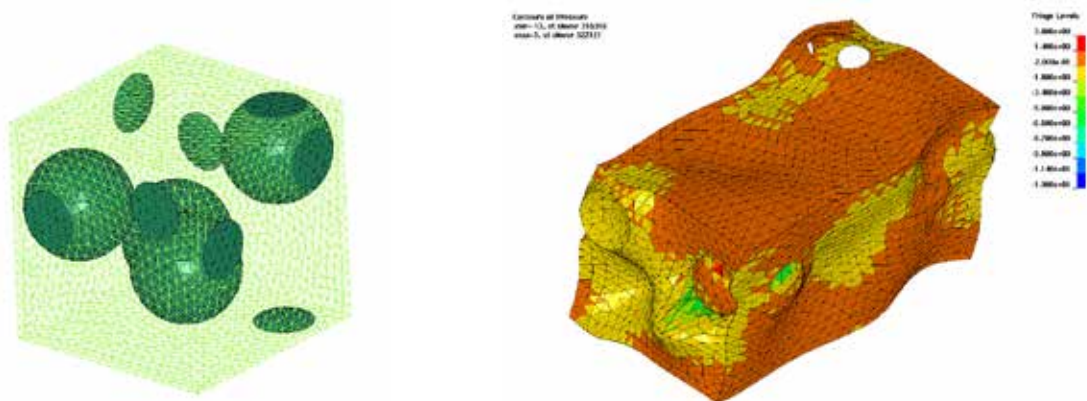
- (1) Multiple PBC equations in the same degree of freedom should be defined under the same group ID. For example, all PBC equations in x direction are defined in the keyword \*CONSTRAINED\_MULTIPLE\_GLOBAL using group ID 1.
- (2) LS-DYNA supports user-define element type, where there can be more than 3 nodal DOFs. In this case, the DOF of RVE nodes in PBC definition should be  $-(i-3)$ , where  $i$  is the global one. The control nodes are usually standard with only three DOFs in 3D. We

recommend to define unique control node for the PBC equation on every global DOF. For example, when using standard solid elements in RVE, we define three control nodes for PBC equations in x, y and z directions, respectively; when using user-defined element type with 7 nodal DOFs, we define 7 control nodes accordingly.

In practice, RVE often contains large number of elements and nodes for modeling the fine details of microstructure. For example, a RVE in material design analysis may have 100x100x100 elements where the number of PBC equations is more than 10 thousand. We developed the keyword `*INCLUDE_UNITCELL` to automatically define PBC equations in LS-DYNA:

- (1) Prepare the RVE mesh in a separated keyword file, e.g. mesh.k
- (2) Include mesh.k through `*INCLUDE_UNITCELL` in the main keyword file
- (3) Define the control nodes starting from card 5 in `*INCLUDE_UNITCELL`
- (4) Run LS-DYNA to generate a new include file, called uc\_mesh.k, where all the PBC equations are automatically defined using `*CONSTRAINED_MULTIPLE_GLOBAL`

Here is an example of particle-reinforced rubber design analysis. The left figure below shows the demo model, where the matrix is rubber material and the spherical parts are the inclusions with much higher stiffness. By imposing PBC and prescribed displacement field, the rubber matrix deforms severely shown in the right figure below, where there is strong stress concentration near the interface between the matrix and inclusions. Based on the periodic assumption, the force-displacement result using RVE can well represent the material behavior and be applied to structure analysis in macro scale.



\* Dr. C.T.Wu graduated from the department of mechanical engineering in University of Iowa in 1999. His expertise is in advanced FEM and meshless methods. He joined LSTC in 2001,

and has been working on the research and development for the solid and structure analysis.

\* Dr. W. Hu graduated from the department of civil engineering in UCLA in 2007, and joined LSTC in 2009. He has been working on the research and development of adaptivity and meshless methods.

## Improvement of Sandwich Structure Part Adaptivity in LS-DYNA

Xinhai Zhu, Houfu Fan, Li Zhang and Yuzhong Xiao  
LSTC

### INTRODUCTION

Mesh adaptivity on sandwich structure part has been implemented in LS-DYNA® for a while. However, the original implementation can only handle sandwich structure part with one layer of solid element, and its usage has been very limited. In this work, the original implementation is successfully extended to multilayer solids, and this feature can be activated with a newly added parameter IFSAND in the keyword \*CONTROL\_ADAPTIVE.

It is demonstrated through a benchmark example that mesh adaptivity on sandwich structure part works very well, and it can provide more detailed fringe contour resolution, for example, at rounded punch corners, while keeping the computational cost at an acceptable level.

### Adaptive Mesh Fission for Sandwich Structure Part

A sandwich structure part consists of two layers of shells each at top and bottom and a core of solid elements in between. As adaptive mesh fission for shells are quite mature in LS-DYNA, the key for the adaptivity of sandwich structure part is the mesh fission scheme for the solid, which is accomplished by making use of the corresponding adaptive mesh of the shells. For instance, if the two shells are discretized into quadrilateral elements and the solid into hexahedral ones, the solid can be adaptively refined by sweeping the corresponding top and bottom adaptive shell through the thickness direction, as shown in Figure 1. If the shells are discretized into triangular elements and the solids are discretized into wedge elements, then the shells can be adaptively refined as more triangular elements and solids refined as more wedge elements (not shown in the Figure).

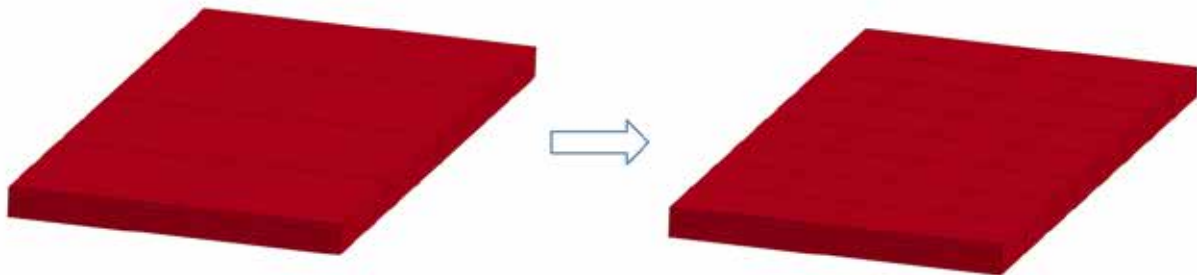


Figure 1. Mesh Fission for Sandwich Structure Part: 32 hexahedral elements are refined to 128 of the same type, as a sweeping of the top and bottom adaptive shell elements through the thickness. The number of layers of the solids always remains the same.

## Activating the New Feature

The mesh adaptivity for multilayer solid core of sandwich structure part can be activated by using a new option in the existing keyword `*CONTROL_ADAPTIVE`, as shown in the following keyword:

```
*CONTROL_ADAPTIVE
$  ADPFREQ    ADPTOL    ADPOPT    MAXLVL    TBIRTH    TDEATH    LCADP    IOFLAG
    0.50      4.0      1         4         0.0      .0006      0        1
$  ADPSIZE    ADPASS    IREFLG    ADPENE    ADPTH    MEMORY    ORIENT    MAXEL
    1.5       1         0         8.000    0.0      MEMORY    ORIENT    MAXEL
$  IADPN90    IADPGH    NCFREQ    IADPCL    ADPCTL    CBIRTH    CDEATH    LCLVL
    -1
$  CNLA                                           IFSAND
                                           1
```

In the keyword, the common adaptive parameters directly apply to the adaptivity of the sandwich structure part. For instance, `ADPFREQ` defines adaptive fission frequency, `ADPTOL` defines the fission tolerance and `ADPOPT` defines the fission option. When the option **IFSAND** is set to be 1, the feature is invoked. Adaptive fusion feature is not yet available for the sandwich structure part.

## Numerical Example and Discussion

To test the new feature, a number of simulations were carried out using the NUMISHEET '96 S-rail Benchmark, as shown in Figure 2. For each case, a forming process is first conducted without adaptive mesh refinement, followed by a corresponding one with adaptive mesh fission.

In the first case, the solid is discretized into one layer of hexahedral elements and the shells are discretized into quadrilateral elements, respectively. The contours of the effective plastic strains at the end of the forming processes with and without adaptive mesh fission are shown in Figure 3. Although the difference of the maximum effective plastic strains in the solid are very small (0.5330 without mesh fission and 0.5469 with fission), the contours with adaptive fission is clearly more localized around the corner areas. This is as expected, given that the newly generated small elements around the corner areas shall provide higher resolutions to the local fringe contours.

In the second case, we would like to consider the solid discretized into multiple (in this case, three) layers of hexahedral elements. The contours of the effective plastic strains at the end of the forming processes with and without adaptive mesh fission are shown in Figure 4. The maximum effective plastic strains are 0.8348 without mesh fission and 0.9159 with fission. Again the one with adaptive mesh fission is more localized at the corner area. Compared to the result obtained from the first case, the current one provides a more detailed gradient in the thickness direction. In fact, the maximum plastic strains are much higher for the 3 layer cases than those for the one layer cases. It is believed that the multiple layer models provide better result in that the nodes of the solid are not completely restricted by the nodes of the shells on the sandwich, as opposed to

the one layer solid model that inevitably imposes extra constraints to the solid nodes, which is less realistic.

In the third case, the shells are discretized into triangle elements and the solid is discretized into wedge elements, so as to show that the hexahedron is not the only option for the solid in sandwich structure part. The resulting effective plastic strains for the case with and without adaptive mesh fission are shown in Figure 5. The contour results present similar localization trend as those in the previous two cases.

To have a better comparison on the maximum effective plastic strains in the solid obtained from the three different cases, the maximum values are summarized in Table 1. One can see that the maximum effective plastic strain neither relies much on the type of the element, nor does it depend much on whether the adaptivity is on or off. In fact, it seems that the number of layers in the thickness direction mainly determines the maximum magnitude of the effective plastic strain. Specifically in the current examples, the maximum values for one layer of element (Hexahedral or Wedge) are around 0.55, while those for three layers of element are higher than 0.83. However, this does not necessarily mean adaptivity is not important in the simulation. The local distribution patterns of the contours are very different, especially in the corner areas, which is usually the locations of great importance. In all respect, the multi-layer core of solid elements feature, as well as the mesh adaptivity option, are both of great significance in the forming simulation of the sandwich structure part.

To uncover the underlying reason why the effective plastic strain resulting from three layers of solid elements is larger, the two cross sections of the solids from the corresponding sandwich structure parts are plotted in Figure 6. Assume that the two sandwich structure parts are subjected to the same pure bending force, which yields a linear distribution of the effective plastic strain along the thickness direction. As can be seen from Figure 6, the Gauss integration point (red dot) corresponding the maximum effective plastic strain of the three layer model is in general closer to the surface, leading to a higher value even though the deformations of the two models are exactly the same.

## **CONCLUSION:**

A new feature of mesh adaptivity for sandwich structure part is successfully implemented and available for use. The new feature supports the adaptive fission of the solid with multiple layers, as compared to the original restriction that allows only one layer of solid elements. This improvement not only provides more detailed information through more layer of elements in the thickness direction, it also provides more freedom to the material within the solid, i.e., nodes of the solid are no longer solely attached to the shells. On the other hand, the adaptive mesh refinement feature serves to provide better resolution of the simulation results in local area of interest while keeping the computational cost to an acceptable level.

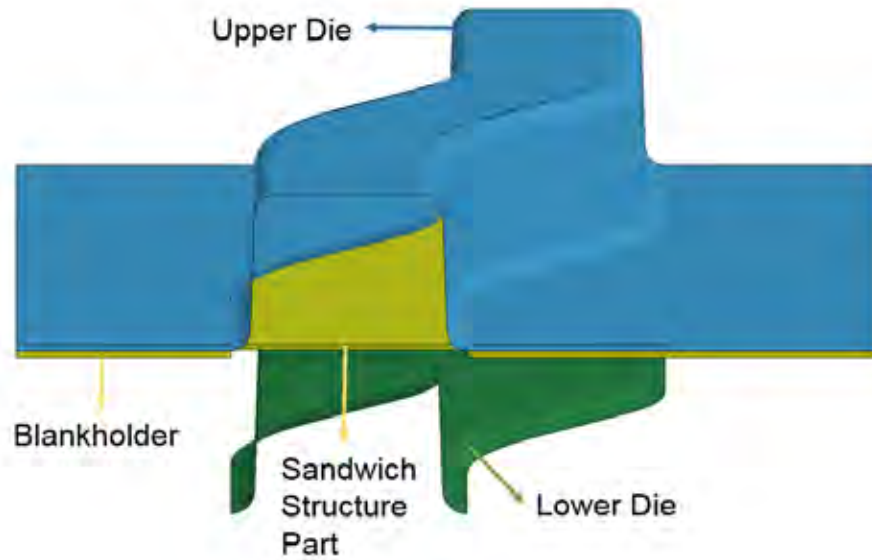


Figure 2. NUMISHEET '96 Benchmark: The upper/lower die and blankholder are rigid; the sandwich structure part consists of one upper, one lower shell and the solid in between. Several forming processes are performed, with different discretization schemes.

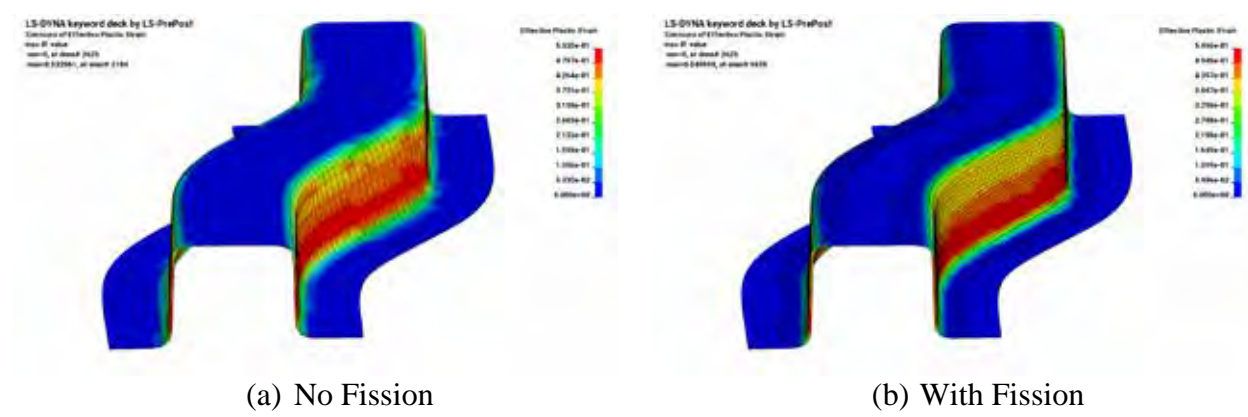
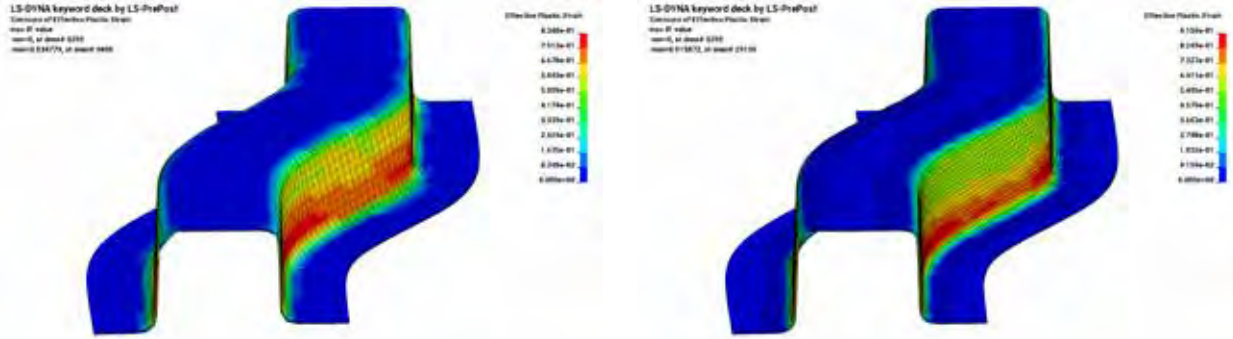


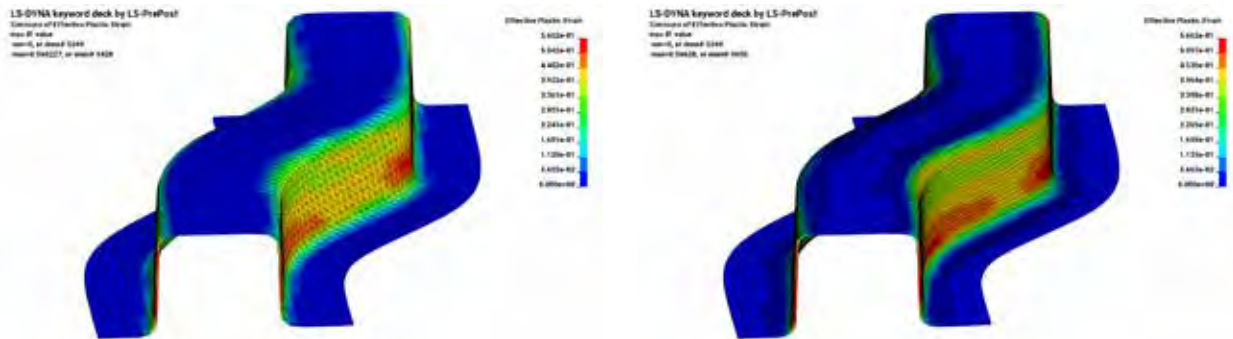
Figure 3. Effective plastic strains of the solid at the end of the forming processes, with and without adaptive fission. The solid is discretized into one layer of hexahedral elements.



(a) No Fission

(b) With Fission

Figure 4. Effective plastic strains of the solid at the end of the forming processes, with and without adaptive fission. The solid is discretized into three layers of hexahedral elements.



(a) No Fission

(b) With Fission

Figure 5. Effective plastic strains of the solid at the end of the forming processes, with and without adaptive fission. The solid is discretized into one layer of wedge elements.

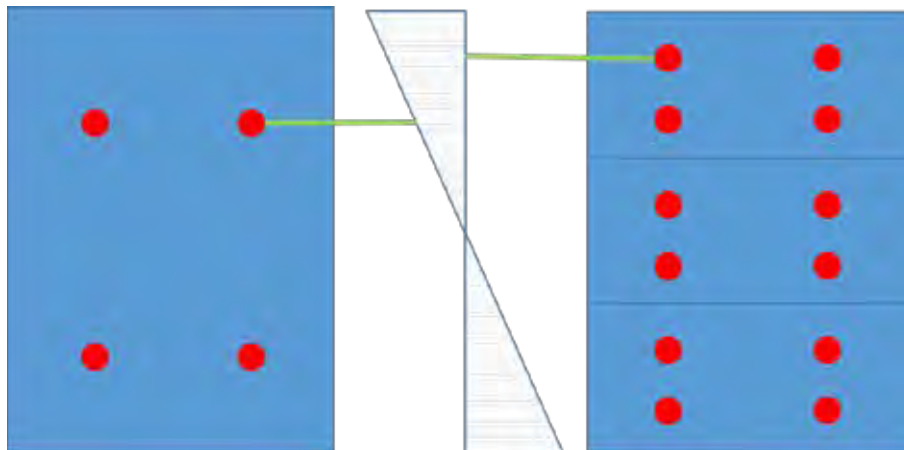


Figure 6. Schematic of the solid cross sections with one and three layers of elements, the dots (red online) denote the locations of Gauss integration points. The two sandwich structure parts are subjected to the same pure bending force. One can easily tell that the one with three layers of elements shall present higher effective plastic strain, simply because the corresponding Gauss integration point is closer to the surface.

	Hex, 1Layer	Hex, 3Layers	Wedge, 1Layer
No Fission	0.5330	0.8348	0.5602
With Fission	0.5496	0.9159	0.5663

Table 1. Comparisons of the final maximum effective plastic strains for the solid meshes of different cases, with and without mesh fission.

### **ACKNOWLEDGEMENT:**

The feature in this article was requested by BMW. Their valuable feedback during the development is highly appreciated.

### **REVISION INFORMATION:**

Sandwich Structure Part Adaptivity feature is available starting in Revision 116282.

## New Inflator Models in LS-DYNA®

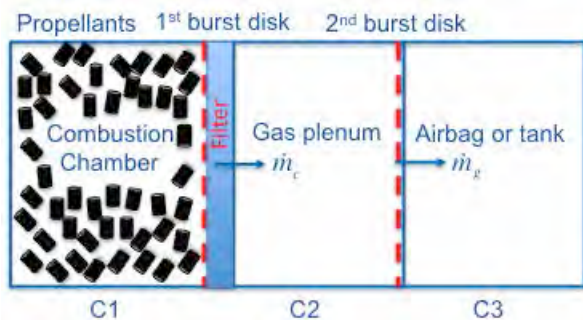
Kyoung-Su Im, Zeng-Chan Zhang, and Grant O. Cook, Jr.  
Livermore Software Technology Corp., Livermore, CA 94551, USA

### Abstract

Three new inflator models for the airbag simulation are developed, i.e., i) the pyrotechnic, ii) the cold flow hybrid, and iii) the heated flow hybrid models. In order to obtain the combustion product gas compositions and the combustion temperature, a PEP (Cruise, 1973) program which is the propellant equilibrium combustion code is also provided. The inflating process is modeled by applying basic conservation laws: the continuity, the energy, and the species transport equations. Unlike other inflator models, here the combustion temperature in these new models is obtained by solving an implicit equation constructed via the thermodynamic relation after the total energy equation is solved. Thus, the new models will be more physical and can provide more accurate results. For user's convenience, three output formats are supported for LS-DYNA's ALE, CPM, and CESE solvers to continue the airbag simulations.

### Introduction

The modeling zones of the pyrotechnic inflator generally consist of the propellant, combustion chamber, gas plenum, and discharge tank. Propellant grains including igniting material are contained and confined to the combustion chamber, which is completely sealed from the rest of the inflator by a thin rupture disk, so that the pressure of the combustion chamber is maintained until it reaches a desired value. Once the propellant is ignited, pressure and temperature will increase rapidly due to combusting propellant grains, and this is followed by the rupture disk opening because of high pressure in the combustion chamber. Then, the filter screen between the combustion chamber and the gas plenum will capture the condensed phase slag, and this also cools the hot gas by permeating through the wide surface area heat sink. When the combustion gas fills in the gas plenum and the pressure in it exceeds a certain specified value, another rupture disk opens and the product gases exhaust into the discharge tank. Since the pressure, temperature and mass flow rate in the discharge tank caused by the performance of the inflator characteristics are the crucial factor in designing an airbag, it is very important for the inflator simulation models to provide accurate information concerning the propellant combustion process.



The schematics of each zone in inflator model.

### Model Descriptions

#### Available Inflator models:

- Pyrotechnic inflator (PI) model: basic model (gas is generated purely by propellant).
- Cold flow hybrid inflator (CFHI) model: inert gas stored in the gas chamber.

- Heated flow hybrid inflator (HFHI) model: the detailed reaction mechanism (currently only gaseous phase) required.

### Basic Assumptions:

- Inflator is divided into several different discrete computational zones: combustion chamber, gas plenum, diffusers, and tank.
- In each zone, the gas and condensed phases are well mixed. Gas phase species are treated as ideal gas while the condensed phase species are incompressible.
- Gas and condensed phases are composed of multiple species with temperature dependent thermodynamics properties. For example, the specific heat for species  $k$  is a function of temperature only, given in terms of a polynomial as,

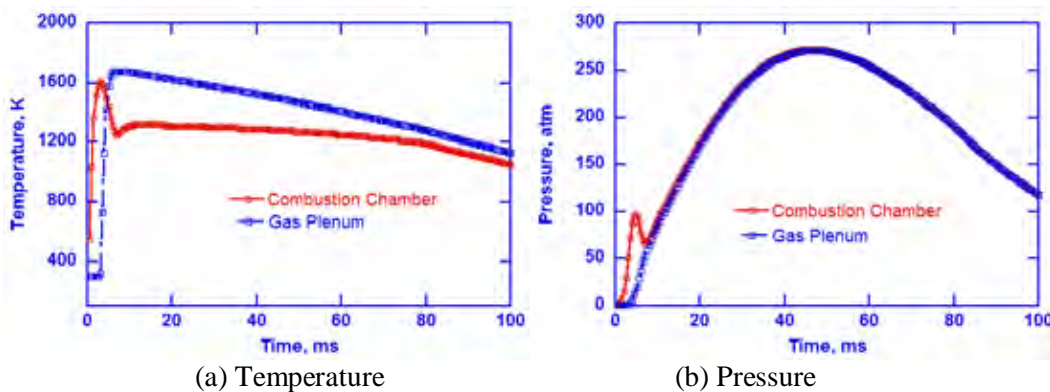
$$\frac{C_{pk}^0}{R} = a_{1k} + a_{2k}T_k + a_{3k}T_k^2 + a_{4k}T_k^3 + a_{5k}T_k^4, \quad C_{ik}^0 = C_{pk}^0 - R_k$$

- The burning rate of the propellant grain is approximated as a function of chamber pressure in time and is converted into the equilibrium compositions. Such compositions can be determined by either an equilibrium code or the stoichiometric combustion reaction.
- The mass flow rates from zone to zone are determined by the gas dynamic formula based on the isentropic flow assumption.

### Calculations:

- In each zone, based on its initial conditions, the continuity, energy, and species transport equations are solved to find the species mass, total energy, chamber pressure, and chamber temperature. (see Fig. a) & b) for example)
- For HFHI model, a detailed mechanism of elementary reaction systems is required in order to compute the species production.

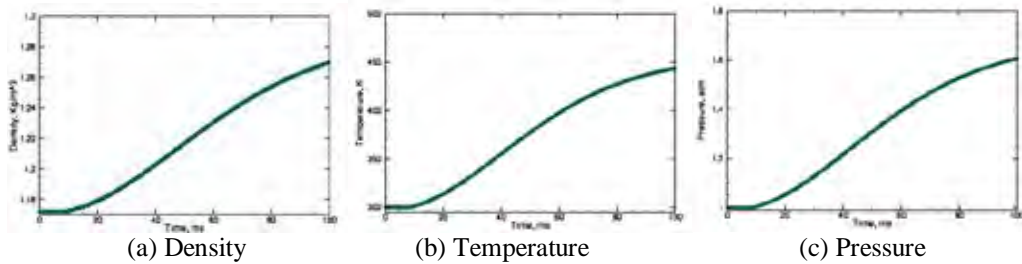
**Fig. a) Combustion & Gas Plenum**



(a) Temperature

(b) Pressure

## b) Discharge Tank



### How to use:

1. Prepare the chemistry input file (\*.inp) and thermodynamics data files (therminf.dat) for participating combustion species in the calculation.
2. Select the inflator model to run.
3. Specify the number of zones (currently, 3 zones only).
4. Set initial conditions for each zone (including the propellant card).
  - a) The combustion chamber: initial conditions, propellant product composition, and chamber compositions.
  - b) If the HFHI model is selected, make sure that the elementary reactions are included in the chemistry input file.
4. Run the code to get the load curve for flow properties.
5. Calibrate the input parameters using experimental data such as the combustion pressure and tank pressure curves.
6. Finally, use the necessary load curves and parameters to continue the airbag simulation

### Remarks:

- The species compositions can be determined by either an equilibrium code or the stoichiometric combustion reaction.
- An LSTC variant of the PEP equilibrium code is provided as a separate code option from LS-DYNA to calculate the combustion species compositions (i.e. mole fractions) and the flame temperature.
- To obtain the accurate input values for the airbag simulation, the pressure curve must be calibrated through a tank test. If possible, it is recommended to conduct pressure curve calibration in the combustion chamber as well.

### References:

1. Butler, P. B., Kang, J., and Krier, H., *Prog. Energy Combust. Sci.*, 19:365-382 (1993).
2. Schmitt, R. G., Butler, P. B., and Jon, J. F., *Combustion Sci. and Tech.*, 122:1-6, 305-330 (1997).
3. Seo, Y.-D. Chung, S. H., and Yoh, J. J., *Fuel*, doi:10.1016/j.fuel.2010.12.042 (2011).
4. O'Loughlin, J. P. and Stevens H. O., "Heated Gas Inflator", US Patent 0290108 (2006).
5. Cruise, D. R., "Theoretical Computations of Equilibrium Compositions, Thermodynamics Properties, and Performance Characteristics of Propellant Systems," PEP Equilibrium Code, Naval Weapons Center Technical Report, NWC TP 6037 (1973).